Advances in Nano Research, *Vol. 16, No. 2 (2024) 201-215*
https://doi.org/10.12989/anr.2024.16.2.201

Sport injury diagnosis of players and equipment via the mathematical simulation on the NEMS sensors

Zishan Wen and Hanhua Zhong*

College of Physical Education, Wuhan University of Technology, Wuhan 430076, Hubei, China

(*Received July 13, 2022, Revised December 28, 2023, Accepted December 29, 2023*)

Abstract. The present research study emphasizes the utilization of mathematical simulation on a nanoelectromechanical systems (NEMS) sensor to facilitate the detection of injuries in players and equipment. Specifically, an investigation is conducted on the thermal buckling behavior of a small-scale truncated conical, cylindrical beam, which is fabricated using porous functionally graded (FG) material. The beam exhibits non-uniform characteristics in terms of porosity, thickness, and material distribution along both radial and axial directions. To assess the thermal buckling performance under various environmental heat conditions, classical and first-order nonlocal beam theories are employed. The governing equations for thermal stability are derived through the application of the energy technique and subsequently numerically solved using the extended differential quadratic technique (GDQM). The obtained results are comprehensively analyzed, taking into account the diverse range of effective parameters employed in this meticulous study.

Keywords: computational investigation; heat resistance; irregular configurations; NEMS; sport application; thermal deformation

1. Introduction

The production of functionally graded materials (FGMs) has also found its way into the world of sports, opening up new possibilities for enhancing athletic performance and equipment design. Functionally graded materials in sports are specifically tailored to meet the demands of athletes, providing improved performance, safety, and comfort. In terms of production, various manufacturing techniques are employed to create functionally graded materials for sports applications (Hou *et al.* 2021, Huang *et al.* 2021b, Xu *et al.* 2021, Wang *et al.* 2022). Advanced composite materials are often utilized, where different fibers or fillers are strategically placed to achieve the desired gradient. For example, in tennis racket production, carbon fibers with different properties can be combined to create a racket frame that offers a gradual transition from increased stiffness at the handle to enhanced flexibility at the racket head. This allows for better control and power transfer during gameplay (Liu *et al.* 2020a, Wang *et al.* 2020, Zhou *et al.* 2020, Dai *et al.* 2021, Guo *et al.* 2021, Shao *et al.* 2021, Wu and Habibi 2021). Additionally, additive manufacturing technologies such as 3D printing have gained popularity in the production of functionally graded sports equipment. This approach enables precise control over material distribution, allowing for the creation of complex and customized designs. For instance, 3D-printed running shoes can incorporate varying levels of cushioning or support along the sole to optimize performance and reduce the risk of injuries. The applications of functionally graded materials in sports are extensive (Fan *et al.* 2023, Miao *et al.* 2023, Qu *et al.* 2023b). In sports equipment, FGMs are employed to improve performance characteristics such as strength, flexibility, and weight distribution. Golf clubs, for example, can be designed with a gradual transition in material properties from the shaft to the clubhead, optimizing energy transfer and enhancing accuracy and distance. Similarly, in skiing and snowboarding, functionally graded materials can be used to create skis and snowboards that offer varying degrees of stiffness along their length, providing better stability and control on different terrains. Moreover, functionally graded materials play a role in sports safety equipment. Helmets for various sports, such as football, cycling, and skiing, can be constructed using FGMs to ensure an optimal balance between impact resistance and comfort (Cao *et al.* 2022, Zhang *et al.* 2022, Cheng *et al.* 2024, Liu *et al.* 2024, Zhao *et al.* 2024). By varying the material properties, helmets can be designed to provide different levels of protection in different regions, reducing the risk of injuries while maintaining wearer comfort.

The thermal stability of functionally graded structures is a critical aspect that influences their performance and reliability in various applications. Functionally graded structures (FGS) are characterized by a gradual variation in composition, microstructure, or material properties, resulting in a smooth transition from one end to another. This unique characteristic enables FGS to exhibit enhanced thermal stability compared to homogeneous materials (Hu *et al.* 2023, Jannat *et al.* 2023, Zhang *et al.* 2023b). One key advantage of functionally graded structures is their ability to mitigate thermal stresses and strains that occur due to temperature gradients. Traditional homogeneous materials are susceptible to thermal expansion and contraction, which can lead to thermal deformation and failure under extreme temperature conditions. In contrast, the graded composition

*Corresponding author, Ph.D.,
E-mail: 8606@whut.edu.cn

ISSN: 2287-237X (Print), 2287-2388 (Online)

and material properties of FGS allow for a better distribution and dissipation of thermal stresses, minimizing the risk of thermal failure. The thermal stability of functionally graded structures can be attributed to several factors. The gradual change in material properties along the gradient helps in reducing the thermal mismatch between adjacent layers, resulting in lower thermal stress concentrations (Di *et al.* 2023, Hou *et al.* 2023b, Li *et al.* 2023b, Zou *et al.* 2023). Additionally, the tailored distribution of materials can optimize thermal conductivity and heat dissipation, preventing the buildup of excessive temperatures in localized regions. The thermal stability of functionally graded structures finds applications in various fields. In aerospace engineering, FGS are employed in the design of components for high-temperature environments, such as turbine blades and thermal protection systems. The graded composition and material properties allow these structures to withstand extreme temperatures while maintaining structural integrity. Furthermore, in the field of energy systems, functionally graded materials are utilized for thermal management and heat transfer applications. FGS can be incorporated into heat exchangers, thermal barriers, and energy storage devices to enhance thermal stability, improve efficiency, and prolong the lifespan of the systems (Liu *et al.* 2020b, Habibi *et al.* 2021, He *et al.* 2021, Huang *et al.* 2021a, Liu *et al.* 2021, Zhang *et al.* 2021). Moreover, functionally graded structures play a crucial role in the development of advanced electronics and microelectron-mechanical systems (MEMS). The thermal stability of FGS is vital in maintaining the performance and reliability of microelectronic devices, such as integrated circuits and sensors, which are subjected to significant thermal fluctuations during operation (Cai *et al.* 2023, Hou *et al.* 2023a, Qu *et al.* 2023a, Zhao *et al.* 2023).

Nanoelectromechanical systems (NEMS) have emerged as a promising technology with potential applications in the sports industry, particularly in the realm of player safety. NEMS devices, which are characterized by their nanoscale size and the integration of mechanical and electrical components, can be utilized to monitor and prevent injuries to athletes in various sports. One key application of NEMS in sports is the development of wearable sensors that can continuously monitor an athlete's vital signs, motion, and impact forces during gameplay. These sensors, often integrated into garments or equipment, can provide real-time data on parameters such as heart rate, body temperature, oxygen levels, and acceleration. By collecting and analyzing this data, coaches, trainers, and medical staff can gain valuable insights into an athlete's physiological state and performance, allowing them to identify potential injury risks or signs of fatigue. This information can then be used to make informed decisions regarding training regimens, rest periods, and injury prevention strategies (He and Deng 2023, Jia *et al.* 2023, Li *et al.* 2023a, Su *et al.* 2023). Another application of NEMS in sports safety is the development of impact sensors that can detect and quantify the magnitude and location of impacts during contact sports. These sensors can be embedded in helmets, mouthguards, or protective padding to provide real-time feedback on the forces experienced by the athlete. By monitoring and analyzing impact data, coaches and medical professionals can identify high-risk situations, assess the effectiveness of protective equipment, and implement strategies to minimize the risk of concussions and other traumatic injuries (Dai *et al.* 2023, Song *et al.* 2023, Yang and Mao 2023, Ye *et al.* 2023). Furthermore, NEMS devices can be utilized in the design and development of smart surfaces and sports equipment with enhanced shock absorption properties. By integrating nanoscale sensors and actuators into sports surfaces or equipment, it becomes possible to dynamically adjust the properties of the surface or equipment based on the detected impact forces. This adaptive capability can help reduce the risk of injuries by providing an optimal level of cushioning and support based on the specific demands of the sport or activity (Jin *et al.* 2023, Lau and Li 2023, Wang *et al.* 2023, Zhang *et al.* 2023d). Additionally, NEMS-based technologies can play a role in the rehabilitation and injury recovery process. Microscale sensors and actuators can be integrated into therapeutic devices, such as braces or joint support systems, to monitor joint movement, muscle activity, and biomechanical parameters. This real-time feedback can assist athletes and medical professionals in optimizing rehabilitation protocols, ensuring proper technique, and preventing reinjury (Cheng *et al.* 2023, Fu *et al.* 2023, Li *et al.* 2023d, Zhang and Huang 2023).

The mathematical simulation of small-scale functionally graded nanoelectromechanical systems (NEMS) sensors and their application in sports offer exciting possibilities for enhancing athlete performance, safety, and monitoring capabilities. By employing mathematical models and simulations, researchers can investigate the behavior and performance of these sensors, which are characterized by their nanoscale size and functionally graded composition (Li 2023, Li *et al.* 2023e, Zhang *et al.* 2023a, c). Functionally graded NEMS sensors can be designed to incorporate varying material properties, such as mechanical stiffness, electrical conductivity, or thermal characteristics, along their structure. Mathematical simulations enable the study of how these graded properties impact the sensor's performance in sports-related applications. One key application of functionally graded NEMS sensors in sports is their integration into wearable devices for athlete monitoring. By employing mathematical models, researchers can simulate the response of these sensors to different mechanical and physiological stimuli (Guan 2023, Li *et al.* 2023c, Ma *et al.* 2023). This enables the prediction of the sensor's sensitivity, accuracy, and range, allowing for the optimization of their design for specific sports applications. For example, simulations can provide insights into how a functionally graded NEMS sensor embedded in a sports garment can accurately measure joint angles, muscle contractions, or impact forces during athletic movements. Mathematical simulations also play a crucial role in assessing the mechanical reliability and durability of functionally graded NEMS sensors. By modeling the stress and strain distribution within the sensor under different loading conditions, researchers can predict potential failure points or areas prone to fatigue. This information can guide the design and fabrication of sensors that can withstand the

rigors of athletic activities, ensuring long-term performance and reducing the risk of sensor failure during sports participation. Furthermore, mathematical simulations enable the exploration of the interaction between functionally graded NEMS sensors and the surrounding environment (Omidi *et al.* 2013, Ghadiri *et al.* 2016c, Mousavi *et al.* 2017). For instance, simulations can evaluate the effects of temperature variations, humidity, or exposure to chemicals on the sensor's performance. This knowledge is valuable in designing sensors that can withstand diverse sports environments, ranging from extreme outdoor conditions to indoor arenas. In sports applications, functionally graded NEMS sensors can be utilized for a variety of purposes. They can monitor an athlete's vital signs, such as heart rate, respiratory rate, or oxygen levels, providing real-time feedback on performance and fatigue levels. The data collected from these sensors can be used to optimize training programs, prevent overexertion, and minimize the risk of injuries. Moreover, functionally graded NEMS sensors can be integrated into sports equipment, such as helmets, protective padding, or footwear, to assess impact forces, detect potential concussions, or provide real-time feedback on technique and performance. Mathematical simulations aid in understanding how these sensors respond to different impact scenarios and can assist in the development of safer sports equipment (Azimi *et al.* 2016, Ghadiri *et al.* 2016a, b, Shafiei *et al.* 2016, 2017).

Many researchers have extensively studied the thermal buckling phenomenon in functionally graded (FG) nanobeams for various applications, with a particular focus on reducing sports-related injuries using NEMS sensors. However, further research is still required, specifically concerning the analysis of nonuniform nanobeams composed of functionally graded materials, particularly in the context of detecting player and equipment injuries using NEMS sensors. This study investigates the thermal buckling behavior of a nonuniform nanobeam made of imperfectly functionally graded materials containing porosity voids. By applying the energy method and employing nonlocal elasticity theory in conjunction with different higher-order beam theories, governing partial differential equations are derived and subsequently solved using GDQM.

2. Simulation using mathematical models

Functionally graded NEMS sensors, utilized for injury detection in players and equipment, can be mathematically modeled by incorporating Timoshenko and Euler-Bernoulli beam theories along with Eringen nonlocal elasticity using the generalized differential quadrature method (GDQM). The GDQM is a numerical technique employed to discretize and solve differential equations, particularly advantageous for complex systems. The unknown variables, such as deflection and strain, are approximated at specific grid points within the beam domain. The differential equations are then converted into a system of algebraic equations by applying the GDQM approximation. The resulting system is subsequently solved numerically to obtain the response of the functionally graded NEMS sensor, including deflection,

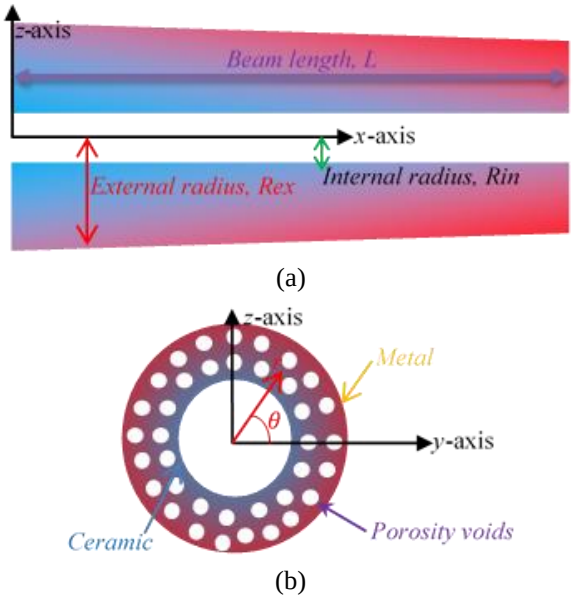

Fig. 1 Depiction of a non-uniform cylindrical nano beam made of functionally graded material, where the porosity distribution affects its properties, (a) schematic of cylindrical beam, (b) cross-section of beam

strain distribution, and thermal buckling load. This combined approach of Timoshenko and Euler-Bernoulli beam theories, Eringen nonlocal elasticity, and the generalized differential quadrature method enables accurate and efficient mathematical modeling of functionally graded NEMS sensors for injury detection in players and equipment.

This paper investigates the thermal buckling behavior of a cylindrical nanobeam composed of a functionally graded material. The material consists of a combination of a metal-based phase and a ceramic phase, with the addition of porosity voids in the radial direction, as illustrated in Fig. 1. The nanobeam has a length denoted as 'L' and is characterized by an internal radius of 'Rin' and an external radius of 'Rex'. Importantly, the external radius varies along the length of the beam in accordance with a mathematical equation.

$$Re\,x_L - Re\,x\,(x) = Re\,x_L\,\alpha\frac{x}{L} \tag{1}$$

where the rate of cross-section change is denoted via '$\alpha = Rex_R/Rex_L$', in which 'Rex_L' is the external radius at 'x=0', and 'Rex_L' is the external radius at 'x=L'.

The FG structure is characterized by a varying material distribution along both the radius and length of the beam, making it a two-dimensional functionally graded (2D-FG) structure. Consequently, the subsequent mathematical equations consider the mechanical properties of elasticity modulus (E), Poisson ratio (ν), and thermal distribution parameter (β) for a porosity-dependent 2D-FG nano cylindrical beam.

$$E = E_{Ceramic} \times \Xi - (E_{Ceramic} - E_{metal})\left(\frac{x}{L}\right)^{\kappa}\left(\frac{r - Rin}{Rex - Rin}\right)^{\mu} \times \Xi \tag{2a}$$

$$\nu = E_{Ceramic} \times \Xi - (\nu_{Ceramic} - \nu_{metal})\left(\frac{x}{L}\right)^{\kappa}\left(\frac{r - R\,i\,n}{R\,e\,x - Rin}\right)^{\mu} \times \Xi \quad (2b)$$

$$\beta = \beta_{Ceramic} \times \Xi - (\beta_{Ceramic} - \beta_{metal})\left(\frac{x}{L}\right)^{\kappa}\left(\frac{r - R\,i\,n}{R\,e\,x - Rin}\right)^{\mu} \times \Xi \quad (2c)$$

In which, the parameter 'κ' represents the FGM value along the length of the beam, 'μ' represents the FGM value along the radius of the beam, and 'Ξ' is the porosity function, which can be defined in the following manner:

$$1 - \Xi = \xi\, cos\left(\frac{r - Rin}{R\,e\,x - Rin}\right) \quad (3)$$

where the parameter 'ξ' is utilized to manage and regulate the porosity voids. The temperature dependency of both the metal and ceramic materials is acknowledged, and their characterization can be described by the equation provided by Touloukian and Ho (1970).

$$\frac{\Re_T}{\Re_0} = \frac{\Re_{-1}}{T} + \Re_1 T + \Re_2 T^2 + \Re_3 T^3 + 1 \quad (4)$$

Within this context, the mechanical parameters denoted as '$\Re_{-1}$', '$\Re_0$', '$\Re_1$', '$\Re_2$', and '$\Re_3$' are temperature-dependent. These parameters are associated with elasticity modulus (E), Poisson ratio (ν), and thermal distribution parameters (β), and their specific values can be found in Table 1.

The thermal buckling behavior of a truncated conical FG nanobeam, which is influenced by porosity, is investigated using both classical beam theory and first-order shear deformation beam theory. In order to accomplish this objective, the energy approach is employed, as described by the equation provided.

$$\delta\Omega + \delta\mho = 0 \quad (5)$$

Where '$\mho$' and 'Ω' are the energy of potential and external work, respectively. In the present study, the external work is equal to zero. The calculation of the virtual potential energy ($\delta\mho$) will be performed in the following manner:

$$\delta\Omega = \iiint \sigma : \varepsilon dV + \iiint \sigma_{ii}\varepsilon_{ii} - \sigma_{ii}\varepsilon^T dV \quad (6)$$

The strains, denoted as 'ε', are defined based on both classical beam theory and the first-order shear deformation beam theory, as follows.

$$\varepsilon_{ij} = \frac{1}{2}\left(u_{j,i} + u_{i,j}\right) \quad (7)$$

Within this context, the displacement fields 'u' along the x-axis (u_x), y-axis (u_y), and z-axis (u_z) are defined as follows.

$$u_x = u + \gamma\left(w_{,x} + \varphi\right) - z w_{,x} \quad (8a)$$

$$u_z = w, u_y = 0 \quad (8b)$$

In this case, the transverse displacement component is represented by 'w', the axial element is denoted as 'u', and the rotation element is indicated as 'φ'. According to the classical beam theory, the value of 'γ' is assumed to be zero. However, based on the first-order shear deformation beam theory, 'γ' is equal to 'z', where '$z = rsin(\theta)$' represents the coordinate along the beam's thickness direction. Moreover, the thermal strains, referred to as 'ε^T', are defined in the following manner.

$$\varepsilon^T + T_0\alpha\left(x, z, T()(x, z, T())\right) \quad (9)$$

In this case, the temperature of a reference point is denoted as 'T_0' with a value of 300K. Additionally, the temperature distribution function, represented as 'T', is defined as follows.

$$T = \Delta T\left(\frac{r - Rin}{R\,e\,x - Rin}\right) + T_0 \quad (10)$$

It should be acknowledged that the strain tensors 'σ' are derived from the provided displacement fields, which are defined as follows.

$$if\, i \neq j \Rightarrow 2\sigma_{ij} = \frac{E\varepsilon_{ij}}{(1+\nu)} \quad (11a)$$

$$if\, i \neq j \Rightarrow \sigma_{ii} = E\varepsilon_{ii} \quad (11b)$$

The nonlocal Eringen theory is a framework that extends the classical beam theories, such as the Timoshenko and Euler-Bernoulli beam theories, by considering the nonlocal effects in the analysis of beams. Unlike the classical theories that assume infinitesimal deformation, the nonlocal Eringen theory accounts for the influence of small-scale material behavior on the overall structural response. This theory introduces a nonlocal parameter that captures the nonlocal interactions between adjacent points along the beam's length. These nonlocal effects become significant at small scales, such as in nanoscale or microscale beams, where the conventional beam theories fail to accurately predict the mechanical behavior. By incorporating nonlocal effects, the Eringen theory provides a more comprehensive and accurate description of the mechanical response of beams, enabling a better understanding and analysis of small-scale structures.

This aligns with nonlocal theory of Eringen (1983), which states that a specific stress field relies on the strain present at all other locations within the body, rather than solely at the reference point. To calculate the complete stress tensors (τ_{ij}), the following procedure needs to be followed:

$$if\, i \neq j \Rightarrow (ea)^2\nabla^2\tau_{ij} - \tau_{ij} = -\frac{E\varepsilon_{ij}}{2(1+\nu)}\varepsilon_{ii}, \quad (12a)$$

$$if\, i \neq j \Rightarrow (ea)^2\nabla^2\tau_{ij} - \tau_{ij} = -E\varepsilon_{ij} \quad (12b)$$

The size-dependent theory is governed by a nonlocal parameter known as 'ea', which plays a crucial role in considering the effects of the structural size on the behavior of the system. This nonlocal parameter is responsible for incorporating the influence of neighboring points and their interactions, allowing the theory to account for length scales

that are comparable to or smaller than the characteristic dimensions of the system. By adjusting the value of '*ea*', the level of nonlocality in the theory can be controlled, enabling a more accurate representation of the size-dependent effects in the structural response. Thus, '*ea*' serves as a key factor in determining the extent to which the size-dependent phenomena are accounted for in the analysis. Subsequently, the nonlocal theory, as expressed in Eqs.(12), is utilized in the evaluation of the virtual potential energy of the strain components, finally, the nonlocal governing equations regarding the energy approach, arising from the various nonlocal strain components is expressed in the following manner:

First-order shear deformation beam theory:

$$\begin{aligned}&\delta(u): \Phi_1 \frac{\partial^2 u}{\partial x^2} + {\Phi_1}' \frac{\partial u}{\partial x} - \Phi_2 \frac{\partial^2 \varphi}{\partial x^2} \\ &= {\Phi_2}' \frac{\partial \varphi}{\partial x} + \Theta' \Delta T \\ &OR \\ &\delta(u): \Theta \Delta T + \Phi_2 \frac{\partial \varphi}{\partial x} - \Phi_1 \frac{\partial u}{\partial x} = 0\end{aligned} \tag{13a}$$

$$\begin{aligned}&\delta(w): \Phi_2 \frac{\partial^2 u}{\partial x^2} - K_S \Phi_4 \left(\frac{\partial w}{\partial x} + \varphi\right) - \\ &\Phi_3 \frac{\partial^2 \varphi}{\partial x^2} + {\Phi_2}' \frac{\partial u}{\partial x} - {\Phi_3}' \frac{\partial \varphi}{\partial x} \\ &+(ea)^2 \Delta T \left(\Theta \frac{\partial^4 w}{\partial x^4} + \Theta''' \frac{\partial w}{\partial x}\right) \\ &+3(ea)^2 \Delta T \left(\Theta' \frac{\partial^3 w}{\partial x^3} + \Theta'' \frac{\partial^2 w}{\partial x^2}\right) \\ &= \Delta T \left(\Theta' \frac{\partial w}{\partial x} + \Theta \frac{\partial^2 w}{\partial x^2}\right) \\ &OR \\ &\delta(w): \Phi_4 \left(\frac{\partial w}{\partial x} + \varphi\right) = \Theta \frac{\partial w}{\partial x} \Delta T\end{aligned} \tag{13b}$$

$$\begin{aligned}&\delta(\varphi): {\Phi_2}' \frac{\partial u}{\partial x} - \Phi_3 \frac{\partial^2 \varphi}{\partial x^2} + \Phi_2 \frac{\partial^2 u}{\partial x^2} \\ &-{\Phi_3}' \frac{\partial \varphi}{\partial x} + \Phi_4 \left(\frac{\partial^2 w}{\partial x^2} + \frac{\partial \varphi}{\partial x}\right) + \Theta' \Delta T \\ &+{\Phi_4}' \left(\frac{\partial w}{\partial x} + \varphi\right) - (ea)^2 \Theta''' \Delta T = 0 \\ &OR \\ &\delta(\varphi): \Phi_3 \frac{\partial \varphi}{\partial x} - \Phi_2 \frac{\partial u}{\partial x} = \Theta \Delta T\end{aligned} \tag{13c}$$

Classical beam theory:

$$\begin{aligned}&\delta(u): \Phi_1 \frac{\partial^2 u}{\partial x^2} - \Phi_2 \frac{\partial^3 w}{\partial x^3} + {\Phi_1}' \frac{\partial u}{\partial x} \\ &= {\Phi_2}' \frac{\partial^2 w}{\partial x^2} + \Theta' \Delta T \\ &OR \\ &\delta(u): \Theta \Delta T + \Phi_2 \frac{\partial^2 w}{\partial x^2} = \Phi_1 \frac{\partial u}{\partial x}\end{aligned} \tag{13d}$$

$$\begin{aligned}&\delta(w): \Phi_2 \frac{\partial^3 u}{\partial x^3} - \Phi_3 \frac{\partial^4 w}{\partial x^4} + 2{\Phi_2}' \frac{\partial^2 u}{\partial x^2} \\ &+{\Phi_2}'' \frac{\partial u}{\partial x} - {\Phi_3}'' \frac{\partial^2 w}{\partial x^2} + 2\Phi_3 \frac{\partial^3 w}{\partial x^3} = \\ &\Theta \frac{\partial^2 w}{\partial x^2} \Delta T + \Theta' \frac{\partial w}{\partial x} \Delta T - (ea)^2 \Theta'' \frac{\partial^2 w}{\partial x^2} \Delta T \\ &-(ea)^2 \Theta''' \frac{\partial w}{\partial x} \Delta T - (ea)^2 \Theta'''' \frac{\partial^4 w}{\partial x^4} \Delta T \\ &-3(ea)^2 \Theta' \frac{\partial^3 w}{\partial x^3} \Delta T + \bar{\Theta}'' \Delta T - (ea)^2 \bar{\Theta}'''' \Delta T \\ &OR \\ &\delta(w): {\Phi_2}' \frac{\partial u}{\partial x} + \Phi_2 \frac{\partial^2 u}{\partial x^2} - \Phi_3 \frac{\partial^3 w}{\partial x^3} \\ &= {\Phi_3}' \frac{\partial^2 w}{\partial x^2} + \Theta \frac{\partial w}{\partial x} \Delta T + \bar{\Theta} \Delta T \\ &OR \\ &\delta\left(\frac{\partial w}{\partial x}\right): \Phi_2 \frac{\partial u}{\partial x} + \Theta \Delta T = \Phi_3 \frac{\partial^2 w}{\partial x^2}\end{aligned} \tag{13e}$$

where

$$\begin{aligned}\Phi_1 &= \iint E r dr d\theta \\ \Phi_2 &= \iint E r^2 \sin(\theta)\, dr d\theta \\ \Phi_3 &= \iint E r^3 \sin^2(\theta)\, dr d\theta \\ \Phi_4 &= \iint K_S \frac{E}{2(1+\nu)} r dr d\theta \\ \Theta &= \iint E \beta r dr d\theta \\ \bar{\Theta} &= \iint E \beta r^2 \sin(\theta)\, dr d\theta\end{aligned} \tag{14a}$$

The shear correction factor, denoted as 'K_S' is typically determined in the following manner for cylindrical beam structures.

$$K_S = 1 + \frac{6}{10}\left(\frac{d}{t}\right)^{0.5} + \frac{1}{4}\left(\frac{d}{t}\right) \tag{14b}$$

where '$d = 2Rex$' is the outer diameter of the pipe and '$t = Rex - Rin$' is the wall thickness. This equation is commonly used to account for the shear deformation effects in pipe structures

3. Solution procedure

The generalized differential quadrilateral method effectively addresses the thermal buckling phenomenon by incorporating both the first-order shear deformation beam theory and classical beam theory within the framework of non-local elasticity theory. This innovative approach combines the advantages of these two theories to provide a comprehensive solution. By considering the non-local effects, the method accurately captures the influence of small-scale thermal disturbances on the buckling behavior of beams. It successfully accounts for the size-dependent effects that classical beam theory fails to address, thereby improving the accuracy of the analysis. The generalized differential quadrilateral method represents a significant advancement in understanding and predicting the thermal buckling of beams, bridging the gap between different

theoretical frameworks and providing a more comprehensive understanding of this complex phenomenon (Ehyaei *et al.* 2017, Ghadiri *et al.* 2017a, b, Shivanian *et al.* 2017).

The generalized differential quadrilateral method effectively solves eigenvalue problems by employing a specialized numerical technique. It discretizes the domain into quadrilateral elements and employs differential operators to express the governing equations. This method accurately captures the eigenvalues of the system by considering higher-order effects and accurately modeling the geometry and boundary conditions. Through the combination of numerical discretization and differential operators, the generalized differential quadrilateral method provides reliable solutions to eigenvalue problems in a computationally efficient manner (Ebrahimi *et al.* 2017, Ghadiri *et al.* 2017c, Shahabinejad *et al.* 2018, Shafiei *et al.* 2020).

The GDQM states that the p^{th}-order derivative functions ($\frac{\partial^p f}{\partial x^p}$) will be transformed into mathematical matrices, which are then combined into a single matrix. The eigenvalues of this final matrix represent the temperature-induced buckling behavior in this particular problem. The GDQM presents a mathematical formulation for the eigenvalue problem associated with the thermal buckling of nanobeams.

First-order shea deformation beam theory:

$$\{[K]-\Delta T[M]\}\begin{Bmatrix}u\\ \varphi\\ w\end{Bmatrix}=0 \tag{15a}$$

Classical beam theory

$$\{[K]-\Delta T[M]\}\begin{Bmatrix}u\\ w\end{Bmatrix}=0 \tag{15b}$$

In which '[*K*]' is the stiffness matrices and '[*M*]' is the mass matrices calculated according to the governing equations. Generalized Differential Quadrilateral Method provides a specific definition for the weighting coefficient corresponding to various orders of derivative functions. In this method, the weighting coefficient serves as a crucial factor in the calculation process. It assigns different importance or influence to the derivative functions based on their respective orders. By appropriately defining the weighting coefficient, the GDQM can effectively account for the varying degrees of significance associated with different orders of derivative functions. This approach allows for a more accurate and comprehensive analysis of the problem at hand, considering the specific characteristics and behaviors of each derivative function.

$$\frac{\partial^t f}{\partial x^t}=\sum_{j=1}^{n}\aleph_{ij}{}^{(t)}= \sum_{j=1}^{n}\left[\aleph_{ij}{}^{(1)}\aleph_{ij}{}^{(t-1)}+\aleph_{ij}{}^{(t-1)}\left(x_j-x_i\right)\right]t \tag{16a}$$

The higher-order derivative functions can be determined by utilizing the lower-order functions. Specifically, the calculation of the first-order derivative can be achieved by following the subsequent procedure:

$$\sum_{j=1}^{n}\aleph_{ij}{}^{(1)}=\sum_{j=1}^{n}\frac{\Psi(x_i)}{\Psi(x_j)(x_i-x_j)} \tag{16b}$$

where

$$\Psi(x_i)=\prod_{j=1,i\neq j}^{n}\left(x_i-x_j\right) \tag{16c}$$

In these equations, the grid point number '*n*' is determined based on the Chebyshev-Gauss-Lobatto approach. This approach involves a specific method for selecting the grid points to ensure accurate and efficient calculations. The Chebyshev-Gauss-Lobatto approach places emphasis on distributing the grid points in a way that optimizes the accuracy of the computations. By employing this approach, the grid points are strategically positioned to minimize errors and enhance the overall performance of the calculations. This careful selection of grid points based on the Chebyshev-Gauss-Lobatto approach ensures reliable and precise results in the equations being considered.

$$2\frac{x_i}{L}=1-cos\left(\frac{i-1}{n-1}\pi\right) \tag{16d}$$

By utilizing the GDQM, the following set of eigenvalue equations is derived from the governing equations. The GDQM approach is applied to transform the governing equations into a formulation that facilitates the determination of eigenvalues. This technique allows for a comprehensive analysis of the system, enabling the calculation of eigenvalues that correspond to the specific characteristics and behavior of the system under consideration.

First-order shear deformation beam theory:

$$\delta(u):\Phi_1\sum_{j=1}^{n}\aleph_{ij}{}^{(2)}u_j+\Phi_1{}'\sum_{j=1}^{n}\aleph_{ij}{}^{(1)}u_j-\Phi_2\sum_{j=1}^{n}\aleph_{ij}{}^{(2)}\varphi_j=\Phi_2{}'\sum_{j=1}^{n}\aleph_{ij}{}^{(1)}\varphi_j+\Theta'\Delta T \tag{17a}$$

$$\begin{aligned}&\delta(w):\Phi_2\sum_{j=1}^{n}\aleph_{ij}{}^{(2)}u_j-\Phi_3\sum_{j=1}^{n}\aleph_{ij}{}^{(2)}\varphi_j\\&-K_S\Phi_4\left(\sum_{j=1}^{n}\aleph_{ij}{}^{(1)}w_j+\varphi_j\right)\\&+\Phi_2{}'\sum_{j=1}^{n}\aleph_{ij}{}^{(1)}u_j-\Phi_3{}'\sum_{j=1}^{n}\aleph_{ij}{}^{(1)}\varphi_j\\&+(ea)^2\Delta T\left(\Theta\sum_{j=1}^{n}\aleph_{ij}{}^{(4)}w_j+\Theta'''\sum_{j=1}^{n}\aleph_{ij}{}^{(1)}w_j\right)\\&+3(ea)^2\Delta T\left(\Theta'\sum_{j=1}^{n}\aleph_{ij}{}^{(3)}w_j+\Theta''\sum_{j=1}^{n}\aleph_{ij}{}^{(2)}w_j\right)\\&=\Delta T\left(\Theta'\sum_{j=1}^{n}\aleph_{ij}{}^{(1)}w_j+\Theta\sum_{j=1}^{n}\aleph_{ij}{}^{(2)}w_j\right)\end{aligned} \tag{17b}$$

$$\delta(\varphi): \Phi_2{}' \sum_{j=1}^{n} \aleph_{ij}{}^{(1)} u_j - \Phi_3 \sum_{j=1}^{n} \aleph_{ij}{}^{(2)} \varphi_j + \Phi_4 \left(\sum_{j=1}^{n} \aleph_{ij}{}^{(2)} w_j + \sum_{j=1}^{n} \aleph_{ij}{}^{(1)} \varphi_j \right) + \Theta' \Delta T + \Phi_2 \sum_{j=1}^{n} \aleph_{ij}{}^{(2)} u_j - \Phi_3{}' \sum_{j=1}^{n} \aleph_{ij}{}^{(1)} \varphi_j + \Phi_4{}' \left(\sum_{j=1}^{n} \aleph_{ij}{}^{(1)} w_j + \varphi_j \right) - (ea)^2 \Theta''' \Delta T = 0 \quad (17c)$$

Classical beam theory:

$$\delta(u): \Phi_1 \sum_{j=1}^{n} \aleph_{ij}{}^{(2)} u_j - \Phi_2 \sum_{j=1}^{n} \aleph_{ij}{}^{(3)} w_j + \Phi_1{}' \sum_{j=1}^{n} \aleph_{ij}{}^{(1)} u_j = \Phi_2{}' \sum_{j=1}^{n} \aleph_{ij}{}^{(2)} w_j + \Theta' \Delta T \quad (17d)$$

$$\delta(w): \Phi_2 \sum_{j=1}^{n} \aleph_{ij}{}^{(3)} u_j - \Phi_3 \sum_{j=1}^{n} \aleph_{ij}{}^{(4)} w_j + 2\Phi_2{}' \sum_{j=1}^{n} \aleph_{ij}{}^{(2)} u_j + \Phi_2{}'' \sum_{j=1}^{n} \aleph_{ij}{}^{(1)} u_j - \Phi_3{}'' \sum_{j=1}^{n} \aleph_{ij}{}^{(2)} w_j + 2\Phi_3 \sum_{j=1}^{n} \aleph_{ij}{}^{(3)} w_j = \Theta \sum_{j=1}^{n} \aleph_{ij}{}^{(2)} w_j \Delta T + \Theta' \sum_{j=1}^{n} \aleph_{ij}{}^{(1)} w_j \Delta T - (ea)^2 \Theta'' \sum_{j=1}^{n} \aleph_{ij}{}^{(2)} w_j \Delta T - (ea)^2 \bar{\Theta}'''' \Delta T - (ea)^2 \Theta''' \sum_{j=1}^{n} \aleph_{ij}{}^{(1)} w_j \Delta T - (ea)^2 \Theta'''' \sum_{j=1}^{n} \aleph_{ij}{}^{(4)} w_j \Delta T - 3(ea)^2 \Theta' \sum_{j=1}^{n} \aleph_{ij}{}^{(3)} w_j \Delta T + \bar{\Theta}'' \Delta T \quad (17e)$$

Subsequently, the governing equation is subjected to the application of boundary conditions. This involves incorporating the specific conditions that govern the behavior of the system at its boundaries. By considering these boundary conditions, the equation is further refined and tailored to accurately model the thermal buckling phenomenon. Solving the resulting equations (Eqs. (17)), yields the eigenvalues associated with the temperature field during thermal buckling. These eigenvalues provide crucial information regarding the critical temperature thresholds and modes of deformation that the system may exhibit. By obtaining these eigenvalues, a deeper understanding of the thermal buckling behavior can be attained, aiding in the design and analysis of structures subjected to thermal loading.

Table 2 Comparison of the presented results for the temperature-induced thermal buckling ($\Delta T/\pi$) of a simply supported nanobeam with the findings of Shan and Huang (2022), considering variations in the nonlocal parameter (ea) and aspect ratio (L/thickness)

	(ea)=0	(ea)=1 (nm)	(ea)=2 (nm)	(ea)=3 (nm)
L/h=40				
Shan and Huang (2022)	22.6896	20.6514	18.9492	17.5062
Present, FSBT	22.6919	20.6535	18.9511	17.508
Present, CBT	22.6862	20.6483	18.9463	17.5036
L/h=50				
Shan and Huang (2022)	14.5298	13.674	12.9071	12.2217
Present, FSBT	14.5313	13.6753	12.9084	12.2229
Present, CBT	14.5276	13.6719	12.9051	12.2198
L/h=60				
Shan and Huang (2022)	10.0933	9.66921	9.27927	8.91958
Present, FSBT	10.0944	9.67017	9.2802	8.92047
Present, CBT	10.0918	9.66772	9.27785	8.91821

4. Analysis and interpretation of the findings

This study investigates the thermal buckling behavior of a small-scale truncated conical, cylindrical beam made of porous functionally graded (FG) material. The beam's non-uniform characteristics in terms of porosity, thickness, and material distribution are examined in both radial and axial directions. Classical and first-order nonlocal beam theories are utilized to evaluate the thermal buckling performance under environmental heat conditions. The governing equations for thermal stability are derived using the energy technique and solved numerically with the extended differential quadratic technique (GDQM). The obtained results are then analyzed in-depth, considering the various effective parameters employed in the study.

In order to validate the numerical results obtained using both the nonlocal classical beam theory (CBT) and first-order shear deformation beam theory (FSDT), a comparison is made with the results presented by Shan and Huang (2022) in Table 2. Shan and Huang (2022) focused on the thermal buckling analysis of rectangular nanobeams using classical beam theory coupled with the nonlocal theory. The comparison involves different nonlocal parameters (*ea*) and various aspect ratios (L/h). It is important to note that Shan's study investigated rectangular geometry, while the current study focuses on cylindrical beams. In the cylindrical structures considered in this study, the beam thickness 'h' is defined as '$h = Rex - Rin$'. The comparison conducted between the numerical approach employed in this study and the generation of governing equations, along with the results obtained, provides robust confirmation of their accuracy. The findings from this comparative analysis unequivocally demonstrate a high level of agreement between the results obtained through the numerical simulations and the expected outcomes. This

Table 3 Effect of FGM parameters involving both axial parameter (κ) and radial parameter (μ) on the thermal buckling temperature ($\Delta T/\pi$) of FG uniform NEMS made of SUS304/Al_2O_3 versus the different aspect ratio (L/(Rex-Rin)) based on both first-order shear deformation beam theory as well as classical beam theory

	'μ=0'	'μ=1'	'μ=2'	'μ=3'	'μ=4'	'μ=5'
First-order shear deformation beam theory, $L = 50(Rex - Rin)$						
'κ=0'	101.2268	129.9247	147.7654	159.4228	167.6331	173.7317
'κ=1'	137.6984	161.9229	174.7114	182.5051	187.7662	191.563
'κ=2'	156.2695	176.457	186.3433	192.17	196.0258	198.7716
'κ=3'	167.3369	184.6654	192.7331	197.3928	200.441	202.5952
'κ=4'	174.8205	190.0127	196.8211	200.6993	203.217	204.9877
Classical beam theory, $L = 50(Rex - Rin)$						
'κ=0'	101.2525	129.9576	147.8028	159.4632	167.6756	173.7758
'κ=1'	137.7333	161.9639	174.7557	182.5513	187.8138	191.6116
'κ=2'	156.3091	176.5017	186.3905	192.2187	196.0755	198.822
'κ=3'	167.3793	184.7122	192.782	197.4429	200.4918	202.6466
'κ=4'	174.8648	190.0609	196.871	200.7502	203.2685	205.0397
First-order shear deformation beam theory, $L = 25(Rex - Rin)$						
'κ=0'	390.0827	501.4622	570.3157	615.2179	646.8059	670.2512
'κ=1'	530.1602	624.2318	673.6483	703.701	723.9629	738.5725
'κ=2'	601.708	680.1711	718.3925	740.8643	755.7131	766.2762
'κ=3'	644.4638	711.8162	743.0019	760.9661	772.6983	780.9808
'κ=4'	673.4541	732.4725	758.7721	773.7109	783.3924	790.1936
Classical beam theory, $L = 25(Rex - Rin)$						
'κ=0'	390.1815	501.5893	570.4602	615.3737	646.9698	670.421
'κ=1'	530.2946	624.39	673.8189	703.8793	724.1463	738.7596
'κ=2'	601.8605	680.3435	718.5745	741.0521	755.9046	766.4703
'κ=3'	644.6271	711.9965	743.1901	761.1589	772.8941	781.1786
'κ=4'	673.6247	732.6581	758.9644	773.9069	783.5909	790.3938

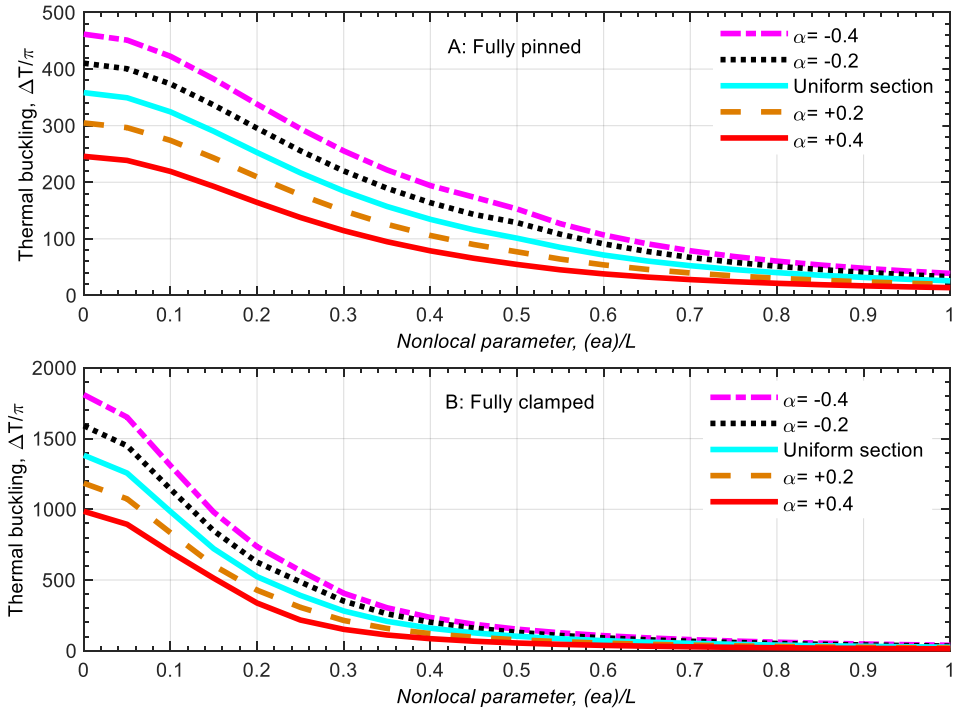

Fig. 2 Impact of nonlocal parameters (*ea*) and geometrical nonuniformity (α) on the thermal buckling of fully clamped and fully pinned FG NEMS, L/Rex_L=30, κ=μ=1

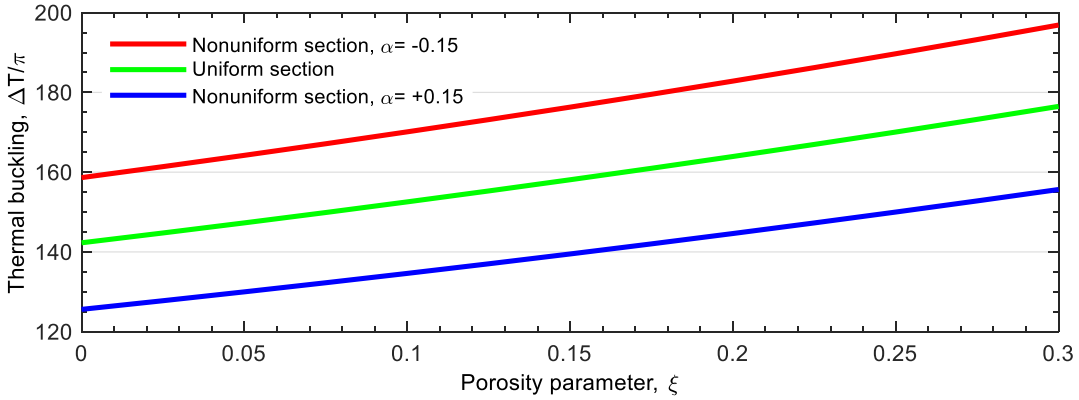

(a) Pure SUS304

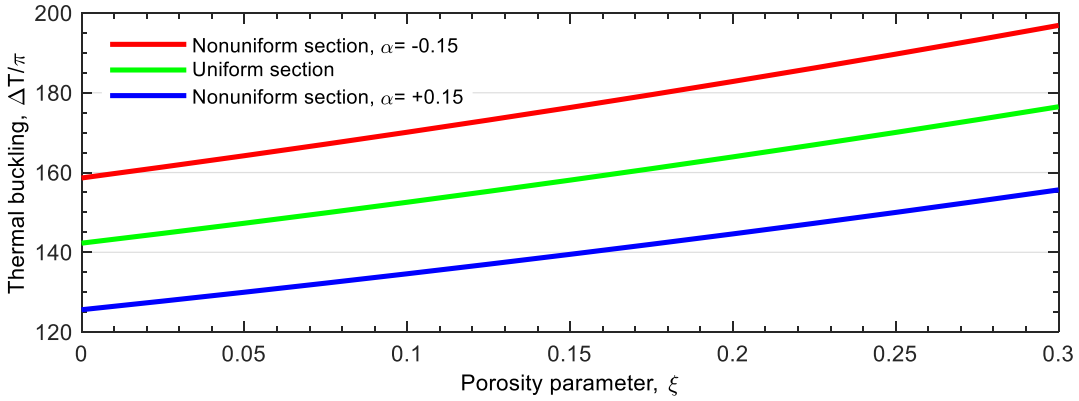

(b) FGM, μ=1

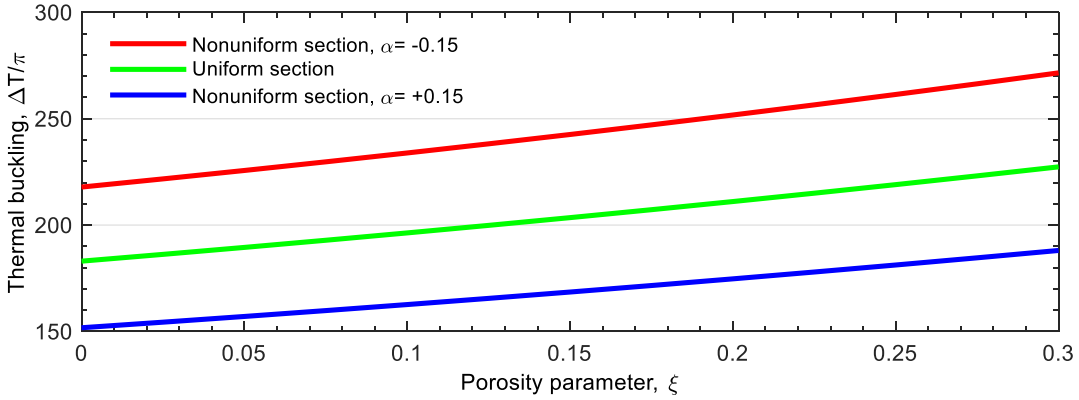

(c) AFGM, κ=1

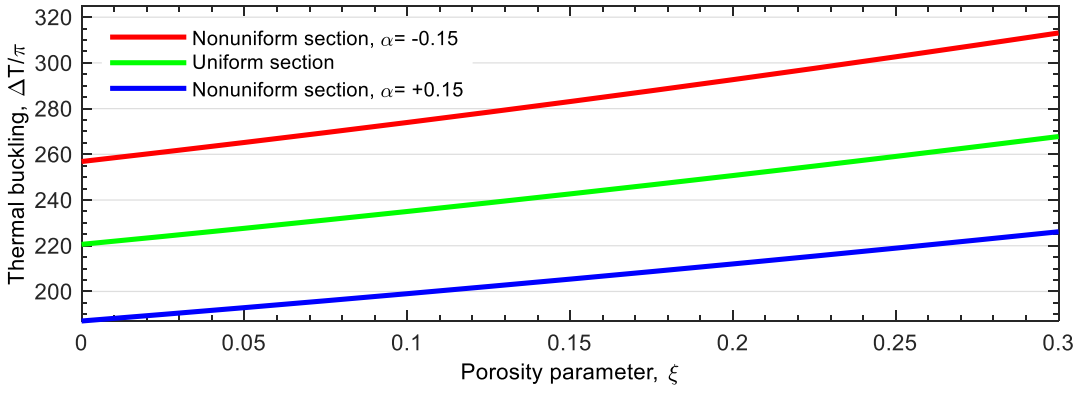

(d) 2DFGM, κ=μ=1

Fig. 3 Effect of porosity parameter along with the rate of cross-section change on the thermal buckling behavior of FG NEMS for different FGM parameters, including the homogeneous, FGM, AFGM, and bi-directional FGM structures made of SUS304/Al_2O_3, L/Rex_L=60, *ea*=0.25L

agreement serves as compelling evidence to support the validity and reliability of the numerical approach and the derived governing equations in accurately capturing and predicting the thermal buckling behavior of the system under investigation. The excellent agreement observed further reinforces the confidence in the obtained results and strengthens the overall credibility of this study's findings.

Within Table 3, a comprehensive compilation is provided, presenting the thermal buckling temperatures ($\Delta T/\pi$) of the FG NEMS sensor fabricated using SUS304/Al_2O_3. The table showcases these temperatures in correlation with the FGM parameters, encompassing both the axial (κ) and radial (μ) directions. Moreover, the thermal buckling temperatures are examined across a range of aspect ratios (L/(*Rex*-*Rin*)) and varying beam theories. By including diverse aspect ratios and beam theories, the table offers a comprehensive analysis of the effects of these factors on the thermal buckling behavior of the FG NEMS sensor. This valuable information facilitates a deeper understanding of the interplay between FGM parameters, aspect ratios, beam theories, and the resulting thermal buckling temperatures, thereby aiding researchers and practitioners in designing and optimizing the performance of FG NEMS sensors. It is noted that the axially functionally graded materials are assumed when the value of 'κ' is nonzero and the 'μ' is equal to zero. Also, the radial FGM means the value of 'κ' equals zero, and 'μ' is nonzero. When comparing the values of thermal buckling between the first-order shear deformation beam theory (FSDT) and the classical beam theory (CBT), several key differences can be observed. The FSDT takes into account the shear deformation effects that occur within the beam, whereas the CBT assumes negligible shear deformation. In general, the FSDT provides more accurate predictions for the thermal buckling behavior of beams, particularly when the aspect ratio (L/h) is large or when the beam is subjected to higher temperatures. This is because the FSDT incorporates shear deformation effects that become more significant under these conditions. On the other hand, the CBT is often considered a simplification of the FSDT, neglecting the shear deformation component and assuming a constant cross-section throughout the beam. In some cases, the thermal buckling values predicted by the FSDT and CBT may exhibit noticeable disparities. The CBT tends to yield higher critical buckling temperatures compared to the FSDT, due to the consideration of shear deformation effects. Therefore, when evaluating the thermal buckling of beams, it is important to choose the appropriate beam theory based on the specific characteristics of the beam, such as its geometry, aspect ratio, material properties, and operating conditions. It should be noted that the choice between FSDT and CBT depends on the level of accuracy required for a particular analysis and the computational resources available. While the FSDT offers more accurate predictions, it is computationally more expensive than the CBT. Therefore, researchers and engineers should carefully consider the trade-off between accuracy and computational efficiency when selecting the appropriate beam theory for analyzing the thermal buckling behavior of beams.

The increment of each FGM parameter along the radius (μ) and beam length (κ) results in increased beam stiffness, which has a direct impact on the beam's resistance to thermal buckling. By carefully manipulating the FGM parameters, such as the material composition, porosity, and thickness distribution, the overall structural characteristics of the beam can be tailored to effectively resist thermal buckling. The gradual change in material properties within the FGM structure allows for a smooth transition of mechanical properties along the beam's length and radius. This spatial variation in material composition helps to alleviate stress concentrations and mitigate the potential for premature buckling under thermal loading. The increased beam stiffness achieved through the bi-directional distribution of FGM parameters leads to improved resistance against thermal buckling. As the beam experiences temperature variations, the FGM's enhanced stiffness helps maintain the structural integrity and stability of the beam, minimizing the risk of buckling and maintaining its load-carrying capacity. The controlled variation of FGM parameters in both radial and axial directions ensures a more uniform distribution of stresses and strains, contributing to the overall improvement in the beam's thermal buckling performance. It is important to note that the specific effect of each FGM parameter on thermal buckling behavior may vary depending on their magnitudes and distributions. Proper optimization and selection of FGM parameters are essential to achieve the desired enhancement in thermal buckling resistance. Through systematic analysis and numerical simulations, the influence of different combinations of FGM parameters can be investigated, allowing for the identification of optimal configurations that maximize the beam's thermal buckling resistance and operational efficiency.

The aspect ratio (L/(*Rex*-*Rin*)) of a functionally graded material (FGM) NEMS, which refers to the ratio of its length to thickness, has a significant influence on its thermal buckling behavior. When the aspect ratio is increased, meaning the length becomes much greater than the thickness, the thermal buckling resistance of the FGM NEMS tends to decrease. This is because a larger aspect ratio leads to a lower flexural stiffness and an increased vulnerability to thermal deformations. Consequently, the FGM NEMS becomes more prone to buckling and may experience thermal instability at lower temperatures. On the other hand, reducing the aspect ratio, where the length is closer to the thickness, enhances the thermal buckling resistance of the FGM NEMS. With a smaller aspect ratio, the NEMS exhibits higher flexural stiffness, allowing it to better withstand thermal deformations and resist buckling even at elevated temperatures. Thus, careful consideration of the aspect ratio is crucial during the design and optimization of FGM NEMS to ensure their thermal stability and reliable performance.

Fig. 2 displays the numerical results of the thermal buckling behavior of bi-directional FG NEMS versus the nonlocal parameters (*ea*) as well as geometrical nonuniformity parameters (α) for both clamped and pinned beams. Geometrical nonuniformity, which refers to variations in the shape, dimensions, or geometry of a structure, can have a profound effect on the thermal

buckling temperatures. When a structure exhibits geometrical nonuniformity, such as changes in cross-sectional area, curvature, or thickness along its length, the distribution of stresses and strains becomes uneven under thermal loading. This uneven distribution can lead to localized regions of higher stress concentrations, resulting in reduced thermal buckling temperatures. In these nonuniform regions, the structural elements are more susceptible to buckling due to the localized thermal effects. Conversely, a structurally uniform system with consistent geometry throughout tends to exhibit higher thermal buckling temperatures. The presence of geometrical nonuniformity introduces additional complexities in predicting and analyzing thermal buckling behavior, emphasizing the importance of carefully considering and managing these variations in the design and optimization of structures to ensure their thermal stability and reliable performance.

The nonlocal parameters affect the stiffness of the nanobeam, which in turn influences its resistance to thermal buckling. Higher values of the nonlocal parameter tend to reduce the stiffness in the pre-buckling configuration, leading to a decrease in the first critical thermal buckling load. Conversely, lower values of the nonlocal parameter enhance the stiffness, thereby increasing the critical thermal buckling load. The nonlocal interactions induced by these parameters redistribute stresses and strains across the nanobeam, affecting its thermal buckling behavior. Furthermore, the nonlocal parameter may also influence the dispersion relation at high wave numbers. It is worth noting that the specific impact of nonlocal parameters on the thermal buckling of FG nanobeams may vary depending on the study, as different aspects such as material index, boundary conditions, thermal effects, and geometrical parameters are considered. Therefore, further investigation and analysis are required to fully understand and optimize the role of nonlocal parameters in enhancing the thermal buckling performance of FG nanobeams.

The thermal buckling behavior of fully clamped and fully pinned beams differs due to the variation in their boundary conditions. A fully clamped beam is rigidly supported at both ends, preventing any translational or rotational movement. In contrast, a fully pinned beam allows for rotational movement at both ends while restraining translational motion. These distinct boundary conditions result in different buckling characteristics. In the case of a fully clamped beam, thermal loading induces compressive thermal stresses. In contrast, a fully pinned beam allows for rotation at both ends, resulting in different buckling behavior. Thermal loading induces thermal stresses in the beam, and under certain conditions, these thermal stresses can lead to buckling instability. However, the critical buckling temperature and the buckling mode of a fully pinned beam are influenced by the specific boundary conditions and the interplay between thermal effects and rotational freedom. The post-buckling behavior of a fully pinned beam can vary depending on the applied thermal loading and the structural parameters. In summary, the thermal buckling of a fully clamped beam and a fully pinned beam differs due to their distinct boundary conditions. While both beams can experience buckling instability under thermal loading, the critical buckling temperature, buckling mode, and post-buckling behavior are influenced by the specific boundary conditions and the interplay between thermal effects and rotational freedom.

In Fig. 3, the investigation focuses on examining the influence of porosity and geometric nonuniformity on the thermal stability and thermal buckling behavior of functionally graded nanostructures. The study considers various types of material distributions, including functionally graded materials (FGM) along the radial direction, axially functionally graded materials (AFGM) along the beam length direction, and bi-directional functionally graded structures. The aim is to understand how porosity and changes in the rate of cross-section affect the thermal buckling response in these nanostructures. The research explores the impact of these factors to enhance the understanding of thermal stability in functionally graded nanostructures with different material distributions. Based on the available search results, it is evident that the porosity parameter has an influence on the thermal buckling behavior, but the specific effects can vary depending on the material distribution. The porosity parameter has been observed to play a role in affecting the thermal buckling temperature and the rate of cross-section change in various types of material distributions. These distributions include functionally graded materials (FGM), axially functionally graded materials (AFGM), and bi-directional functionally graded materials structures. One important observation is that the porosity parameter tends to enhance the thermal buckling temperature. In other words, as the porosity parameter increases, the temperature at which thermal buckling occurs also increases. This indicates that the presence of porosity in the material can have a positive effect on its thermal stability and resistance to buckling under thermal loading conditions. On the other hand, it has been noted that the thermal buckling decreases with the rate of cross-section change in the mentioned material distributions. This implies that as the rate of cross-section change increases, the likelihood of thermal buckling occurring decreases. It is worth mentioning that the specific mechanisms and underlying factors responsible for these observations may vary depending on the specific material composition, geometric parameters, and other influencing factors. Further research and analysis are necessary to fully understand and quantify the relationship between the porosity parameter, thermal buckling temperature, and the rate of cross-section change in different material distributions.

5. Conclusions

The primary focus of the present study was to investigate the use of functionally graded (FG) nano-electromechanical systems (NEMS) sensors for sports applications, with the aim of preventing injuries. To achieve this goal, a comprehensive framework was developed, which involved mathematical modeling of an FG NEMS sensor using both first-order shear deformation beam theory

and classical beam theory coupled with the nonlocal Eringen theory. These theories were employed to accurately capture the effects of small-scale impacts and extract the governing nonlocal partial differential equations and associated boundary conditions. The FG NEMS sensor was composed of porosity-dependent materials, specifically SUU304/Al2O3, where the material distributions varied along the length and radial direction of the beam, while porosity voids were distributed along the beam radius. Additionally, the geometry of the NEMS sensor was nonuniform along its length and continuously changed throughout its span. Subsequently, numerical simulations were conducted to analyze the thermal buckling behavior of the nonuniform imperfect FG NEMS sensor. The main conclusions drawn from this research can be summarized as follows:

• The parameters of functionally graded materials (FGMs) in both the radial and axial directions contribute to the enhancement of beam stiffness, thereby improving its structural integrity and resistance to thermal buckling. Additionally, these FGM parameters have a tendency to increase the thermal buckling temperature.

• The inclusion of the nonlocal parameter decreases the beam stiffness, resulting in reduced beam stability and an increased susceptibility to thermal buckling.

• Reducing the rate of cross-section adversely impacts beam stability, resulting in a decrease in thermal buckling resistance.

• The anticipated thermal buckling of the beam with clamped boundary conditions exceeds that of beams with pinned supports, indicating that clamped beams exhibit greater stability compared to pinned beams.

• The thermal buckling of FGM structures is intensified by the presence of the porosity parameter.

Acknowledgment

This work was supported by General Project of National Social Science Foundation (Project No:22BTY015).

References

Azimi, M., Mirjavadi, S.S., Shafiei, N. and Hamouda, A.M.S. (2016), "Thermo-mechanical vibration of rotating axially functionally graded nonlocal Timoshenko beam", *Appl. Phys. A.* **123**(1), 104. https://doi.org/10.1007/s00339-016-0712-5.

Cai, L., Yan, S., Ouyang, C., Zhang, T., Zhu, J., Chen, L., Ma, X. and Liu, H. (2023), "Muscle synergies in joystick manipulation", *Front Physiol*., **14**, 1282295. https://doi.org/10.3389/fphys.2023.1282295.

Cao, C., Wang, J., Kwok, D., Cui, F., Zhang, Z., Zhao, D., Li, M.J. and Zou, Q. (2022), "webTWAS: a resource for disease candidate susceptibility genes identified by transcriptome-wide association study", *Nucl. Acids Res.*, **50**(D1), D1123-D1130. https://doi.org/10.1093/nar/gkab957.

Cheng, F., Niu, B., Xu, N. and Zhao, X. (2024), "Resilient distributed secure consensus control for uncertain networked agent systems under hybrid DoS attacks", *Commun. Nonlinear Sci. Numer. Simul.*, **129**, 107689. https://doi.org/10.1016/j.cnsns.2023.107689.

Cheng, Q., Ali, H.E. and Albaijan, I. (2023), "Optimization of the cross-section regarding the stability of nanostructures according to the dynamic analysis", *Adv. Concr. Constr.*, **15**(4), 215-228. https://doi.org/10.12989/acc.2023.15.4.215.

Dai, Y., Jiang, Z., Chen, K.-y., Zuo, D., Ali, H.E. and Albaijan, I. (2023), "Geometry impact on the stability behavior of cylindrical microstructures: Computer modeling and application for small-scale sport structures", *Steel Compos. Struct.*, **48**(4), 443. https://doi.org/10.12989/scs.2023.48.4.443.

Dai, Z., Jiang, Z., Zhang, L. and Habibi, M. (2021), "Frequency characteristics and sensitivity analysis of a size-dependent laminated nanoshell", *Adv. Nano Res.*, **10**(2), 175. https://doi.org/10.12989/anr.2021.10.2.175.

Di, Y., Li, R., Tian, H., Guo, J., Shi, B., Wang, Z., Yan, K. and Liu, Y. (2023), "A maneuvering target tracking based on fastIMM-extended Viterbi algorithm", *Neural Comput. Appl.*, 1-10. https://doi.org/10.1007/s00521-023-09039-1.

Ebrahimi, F., Shafiei, N., Kazemi, M. and Mousavi Abdollahi, S.M. (2017), "Thermo-mechanical vibration analysis of rotating nonlocal nanoplates applying generalized differential quadrature method", *Mech. Adv. Mater. Struct.*, **24**(15), 1257-1273. https://doi.org/10.1080/15376494.2016.1227499.

Ehyaei, J., Akbarshahi, A. and Shafiei, N. (2017), "Influence of porosity and axial preload on vibration behavior of rotating FG nanobeam", *Adv. Nano Res.*, **5**(2), 141. https://doi.org/10.12989/anr.2017.5.2.141.

Eringen, A.C. (1983), "On differential equations of nonlocal elasticity and solutions of screw dislocation and surface waves", *J. Appl. Phys.*, **54**(9), 4703-4710. https://doi.org/10.1063/1.332803.

Fan, Z., He, Y., Sun, W., Li, Z., Ye, C. and Wang, C. (2023), "Clinical characteristics, diagnosis and management of Sweet syndrome induced by azathioprine", *Clin. Experim. Med.*, **23**(7), 3581-3587. https://doi.org/10.1007/s10238-023-01135-9.

Fu, L., Li, J., Yang, J., Liu, Y., He, C. and Chen, Y. (2023), "Purification process and reduction of heavy metals from industrial wastewater via synthesized nanoparticle for water supply in swimming/water sport", *Adv. Nano Res.*, **15**(5), 441-449. https://doi.org/10.12989/anr.2023.15.5.441.

Ghadiri, M., Hosseini, S.H.S. and Shafiei, N. (2016a), "A power series for vibration of a rotating nanobeam with considering thermal effect", *Mech. Adv. Mater. Struct.*, **23**(12), 1414-1420. https://doi.org/10.1080/15376494.2015.1091527.

Ghadiri, M., Shafiei, N. and Alavi, H. (2017a), "Thermo-mechanical vibration of orthotropic cantilever and propped cantilever nanoplate using generalized differential quadrature method", *Mech. Adv. Mater. Struct.*, **24**(8), 636-646. https://doi.org/10.1080/15376494.2016.1196770.

Ghadiri, M., Shafiei, N. and Alireza Mousavi, S. (2016b), "Vibration analysis of a rotating functionally graded tapered microbeam based on the modified couple stress theory by DQEM", *Appl. Phys. A*, **122**(9), 837. https://doi.org/10.1007/s00339-016-0364-5.

Ghadiri, M., Shafiei, N. and Babaei, R. (2017b), "Vibration of a rotary FG plate with consideration of thermal and Coriolis effects", *Steel Compos. Struct.*, **25**(2), 197-207. https://doi.org/10.12989/scs.2017.25.2.197.

Ghadiri, M., Shafiei, N. and Hossein Alavi, S. (2017c), "Vibration analysis of a rotating nanoplate using nonlocal elasticity theory", *J. Solid Mech.*, **9**(2), 319-337.

Ghadiri, M., Shafiei, N., Salekdeh, S.H., Mottaghi, P. and Mirzaie, T. (2016c), "Investigation of the dental implant geometry effect on stress distribution at dental implant–bone interface", *J. Brazil. Soc. Mech. Sci. Eng.*, **38**(2), 335-343. https://doi.org/10.1007/s40430-015-0472-8.

Guan, S. (2023), "Systematic test on the effectiveness of MEMS nano-sensing technology in monitoring heart rate of Wushu

exercise", *Adv. Nano Res.*, **15**(2), 155-163. https://doi.org/10.12989/anr.2023.15.2.155.

Guo, J., Baharvand, A., Tazeddinova, D., Habibi, M., Safarpour, H., Roco-Videla, A. and Selmi, A. (2021), "An intelligent computer method for vibration responses of the spinning multi-layer symmetric nanosystem using multi-physics modeling", *Eng. Comput.*, 1-22. https://doi.org/10.1007/s00366-021-01433-4.

Habibi, M., Darabi, R., Sa, J.C.d. and Reis, A. (2021), "An innovation in finite element simulation via crystal plasticity assessment of grain morphology effect on sheet metal formability", *Proceedings of the Institution of Mechanical Engineers, Part L: Journal of Materials: Design and Applications*, **235**(8), 1937-1951. https://doi.org/10.1177/14644207211024686.

He, L. and Deng, Q. (2023), "Construction of sports engineering structures with high resistance to improve the quality of sports training", *Struct. Eng. Mech.*, **86**(2), 211-220. https://doi.org/10.12989/sem.2023.86.2.211.

He, X., Ding, J., Habibi, M., Safarpour, H. and Safarpour, M. (2021), "Non-polynomial framework for bending responses of the multi-scale hybrid laminated nanocomposite reinforced circular/annular plate", *Thin Wall. Struct.*, **166**, 108019. https://doi.org/10.1016/j.tws.2021.108019.

Hou, F., Wu, S., Moradi, Z. and Shafiei, N. (2021), "The computational modeling for the static analysis of axially functionally graded micro-cylindrical imperfect beam applying the computer simulation", *Eng. Comput.*, 1-19. https://doi.org/10.1007/s00366-021-01456-x.

Hou, X., Xin, L., Fu, Y., Na, Z., Gao, G., Liu, Y., Xu, Q., Zhao, P., Yan, G., Su, Y., Cao, K., Li, L. and Chen, T. (2023a), "A self-powered biomimetic mouse whisker sensor (BMWS) aiming at terrestrial and space objects perception", *Nano Energy*, **118**, 109034. https://doi.org/10.1016/j.nanoen.2023.109034.

Hou, X., Zhang, L., Su, Y., Gao, G., Liu, Y., Na, Z., Xu, Q., Ding, T., Xiao, L., Li, L. and Chen, T. (2023b), "A space crawling robotic bio-paw (SCRBP) enabled by triboelectric sensors for surface identification", *Nano Energy*, **105**, 108013. https://doi.org/10.1016/j.nanoen.2022.108013.

Hu, Z., Ren, L., Wei, G., Qian, Z., Liang, W., Chen, W., Lu, X., Ren, L. and Wang, K. (2023), "Energy flow and functional behavior of individual muscles at different speeds during human walking", *IEEE T Neural Syst. Rehabil. Eng.*, **31**, 294-303. https://doi.org/10.1109/TNSRE.2022.3221986.

Huang, X., Hao, H., Oslub, K., Habibi, M. and Tounsi, A. (2021a), "Dynamic stability/instability simulation of the rotary size-dependent functionally graded microsystem", *Eng. Comput.*, 1-17. https://doi.org/10.1007/s00366-021-01399-3.

Huang, X., Zhang, Y., Moradi, Z. and Shafiei, N. (2021b), "Computer simulation via a couple of homotopy perturbation methods and the generalized differential quadrature method for nonlinear vibration of functionally graded non-uniform micro-tube", *Eng. Comput.*, 1-18. https://doi.org/10.1007/s00366-021-01395-7.

Jannat, M.K.A., Islam, M.S., Yang, S.H. and Liu, H. (2023), "Efficient Wi-Fi-based human activity recognition using adaptive antenna elimination", *IEEE Access*, **11**, 105440-105454. https://doi.org/10.1109/ACCESS.2023.3320069.

Jia, S., Niu, X., Jia, F. and Mahmoudi, T. (2023), "Advantages and disadvantages of renewable energy-oil-environmental pollution-from the point of view of nanoscience", *Adv. Concr. Constr.*, **16**(1), 69-78. https://doi.org/10.12989/acc.2023.16.1.069.

Jin, H., Zhang, B. and Duan, X. (2023), "Impact of nanocomposite material to counter injury in physical sport in the tennis racket", *Adv. Nano Res.*, **14**(5), 435-442. https://doi.org/10.12989/anr.2023.14.5.435.

Lau, J.-S. and Li, Z. (2023), "Human functions in innovation and sustainable marketing", *Adv. Concr. Constr.*, **16**(2), 97. https://doi.org/10.12989/acc.2023.16.2.097.

Li, J., Bin, N., Guo, F., Gao, X., Chen, R., Yao, H. and Zhou, C. (2023a), "Analysis on the influence of sports equipment of fiber reinforced composite material on social sports development", *Adv. Nano Res.*, **15**(1), 49-57. https://doi.org/10.12989/anr.2023.15.1.049.

Li, S., Chen, H., Chen, Y., Xiong, Y. and Song, Z. (2023), " Hybrid method with parallel-factor theory, a support vector machine, and particle filter optimization for intelligent machinery failure identification", *Machines*, **11**(8), 837. https://doi.org/10.3390/machines11080837.

Li, X., Ali, H.E. and Albaijan, I. (2023c), "TiO 2-containing nanocomposite structure: Application and investigation in shoes sports medical soles in physical activities", *Adv. Nano Res.*, **15**(4), 329-337. https://doi.org/10.12989/anr.2023.15.4.329.

Li, Y., Li, M., Kong, X., Baniasadi, A., Shaker, A.H. and Ali, H.E. (2023d), "Psychological capital to foster employee creativity in nanotechnology companies: the mediating role of JS and CSR", *Adv. Nano Res.*, **15**(3), 277-283. https://doi.org/10.12989/anr.2023.15.3.277.

Li, Z. (2023), "Resistance of concrete made of fibers in weight lifting slabs against impact in sports training", *Struct. Eng. Mech.*, **86**(3), 325-336. https://doi.org/10.12989/sem.2023.86.3.325.

Li, Z., Peng, S. and Chen, G. (2023e), "Research on safety assessment and application effect of nanomedical products in physical education", *Adv. Nano Res.*, **15**(3), 253-261. https://doi.org/10.12989/anr.2023.15.3.253.

Liu, H., Zhao, Y., Pishbin, M., Habibi, M., Bashir, M. and Issakhov, A. (2021), "A comprehensive mathematical simulation of the composite size-dependent rotary 3D microsystem via two-dimensional generalized differential quadrature method", *Eng. Comput.*, 1-16. https://doi.org/10.1007/s00366-021-01419-2.

Liu, S., Niu, B., Karimi, H.R. and Zhao, X. (2024), "Self-triggered fixed-time bipartite fault-tolerant consensus for nonlinear multiagent systems with function constraints on states", *Chaos, Solitons Fract.*, **178**, 114367. https://doi.org/10.1016/j.chaos.2023.114367.

Liu, Z., Su, S., Xi, D. and Habibi, M. (2020a), "Vibrational responses of a MHC viscoelastic thick annular plate in thermal environment using GDQ method", *Mech. Based Des. Struct.*, 1-26. https://doi.org/10.1080/15397734.2020.1784201.

Liu, Z., Wu, X., Yu, M. and Habibi, M. (2020b), "Large-amplitude dynamical behavior of multilayer graphene platelets reinforced nanocomposite annular plate under thermo-mechanical loadings", *Mech. Based Des. Struct.*, 1-25. https://doi.org/10.1080/15397734.2020.1815544.

Ma, Z., Qi, J., Xun, W. and Li, Y. (2023), "Sports injury treatment and sports rehabilitation employing the Nanoparticles containing zinc oxide", *Adv. Nano Res.*, **15**(1), 67-74. https://doi.org/10.12989/anr.2023.15.1.067.

Miao, Y., Wang, X., Wang, S. and Li, R. (2023), "Adaptive switching control based on dynamic zero-moment point for versatile hip exoskeleton under hybrid locomotion", *IEEE T Ind. Electr.*, **70**(11), 11443-11452. https://doi.org/10.1109/TIE.2022.3229343.

Mousavi, S.M., Shafiei, N. and Dadvand, A. (2017), "Numerical simulation of subsonic turbulent flow over NACA0012 airfoil: evaluation of turbulence models", *Sigma J. Eng. Natural Sci.*, **35**(1), 133-155.

Omidi, S., Oskooee, M.B. and Shafiei, N. (2013), "Finite element analysis of an ultra-fine grained Titanium dental implant covered by different thicknesses of hydroxyapatite layer", *Indian J. Dent.*, **4**(1), 1-4. https://doi.org/10.1016/j.ijd.2012.10.002.

Qu, J., Mao, B., Li, Z., Xu, Y., Zhou, K., Cao, X., Fan, Q., Xu, M., Liang, B., Liu, H., Wang, X. and Wang, X. (2023a), "Recent progress in advanced tactile sensing technologies for soft grippers", *Adv. Funct. Mater.*, **33**(41), 2306249. https://doi.org/10.1002/adfm.202306249.

Qu, J., Yuan, Q., Li, Z., Wang, Z., Xu, F., Fan, Q., Zhang, M., Qian, X., Wang, X., Wang, X. and Xu, M. (2023b), "All-in-one strain-triboelectric sensors based on environment-friendly ionic hydrogel for wearable sensing and underwater soft robotic grasping", *Nano Energy*, **111**, 108387. https://doi.org/10.1016/j.nanoen.2023.108387.

Reddy, J.N. and Chin, C.D. (1998), "Thermomechanical analysis of functionally graded cylinders and plates", *J. Therm. Stress.*, **21**(6), 593-626. https://doi.org/10.1080/01495739808956165.

Shafiei, N., Ghadiri, M., Makvandi, H. and Hosseini, S.A. (2017), "Vibration analysis of Nano-Rotor's Blade applying Eringen nonlocal elasticity and generalized differential quadrature method", *Appl. Math. Modell.*, **43**, 191-206. https://doi.org/10.1016/j.apm.2016.10.061.

Shafiei, N., Hamisi, M. and Ghadiri, M. (2020), "Vibration analysis of rotary tapered axially functionally graded Timoshenko nanobeam in thermal environment", *J. Solid Mech.*, **12**(1), 16-32. https://doi.org/10.22034/jsm.2019.563759.1273.

Shafiei, N., Kazemi, M. and Ghadiri, M. (2016), "Nonlinear vibration behavior of a rotating nanobeam under thermal stress using Eringen's nonlocal elasticity and DQM", *Appl. Phys. A.* **122**(8), 728. https://doi.org/10.1007/s00339-016-0245-y.

Shahabinejad, E., Shafiei, N. and Ghadiri, M. (2018), "Influence of temperature change on modal analysis of rotary functionally graded nano-beam in thermal environment", *J. Solid Mech.*, **10**(4), 779-803. https://jsm.arak.iau.ir/article_545719.html.

Shan, X. and Huang, A. (2022), "Intelligent simulation of the thermal buckling characteristics of a tapered functionally graded porosity-dependent rectangular small-scale beam", *Adv. Nano Res.*, **12**(3), 281-290. https://doi.org/10.12989/anr.2022.12.3.281.

Shao, Y., Zhao, Y., Gao, J. and Habibi, M. (2021), "Energy absorption of the strengthened viscoelastic multi-curved composite panel under friction force", *Arch. Civil Mech. Eng.*, **21**(4), 1-29. https://doi.org/10.1007/s43452-021-00279-3.

Shivanian, E., Ghadiri, M. and Shafiei, N. (2017), "Influence of size effect on flapwise vibration behavior of rotary microbeam and its analysis through spectral meshless radial point interpolation", *Appl. Phys. A*, **123**(5), 329. https://doi.org/10.1007/s00339-017-0955-9.

Song, S., Zhang, T. and Zhui, Z. (2023), "Dynamic analysis of nanotube-based nanodevices for drug delivery in sports-induced varied conditions applying the modified theories", *Steel Compos. Struct.*, **49**(5), 487. https://doi.org/10.12989/scs.2023.49.5.487.

Su, Z., Meng, J. and Su, Y. (2023), "Application of SiO_2 nanocomposite ferroelectric material in preparation of trampoline net for physical exercise", *Adv. Nano Res.*, **14**(4), 355-362. https://doi.org/10.12989/anr.2023.14.4.355.

Touloukian, Y.S. and Ho, C. (1970), *Thermal expansion. Nonmetallic solids*, *Thermophysical properties of matter-The TPRC Data Series*, New York, U.S.A.

Wang, G., Peng, K., Zhou, H., Liu, G., Lou, Z. and Pan, F. (2023), "Nanocomposite reinforced structures to deal with injury in physical sports", *Adv. Nano Res.*, **14**(6), 541-555. https://doi.org/10.12989/anr.2023.14.6.541.

Wang, P., Gao, Z., Pan, F., Moradi, Z., Mahmoudi, T. and Khadimallah, M.A. (2022), "A couple of GDQM and iteration techniques for the linear and nonlinear buckling of bi-directional functionally graded nanotubes based on the nonlocal strain gradient theory and high-order beam theory", *Eng. Anal. Bound. Elem.*, **143**, 124-136. https://doi.org/10.1016/j.enganabound.2022.06.007.

Wang, Z., Yu, S., Xiao, Z. and Habibi, M. (2020), "Frequency and buckling responses of a high-speed rotating fiber metal laminated cantilevered microdisk", *Mech. Adv. Mater. Struct.*, 1-14. https://doi.org/10.1080/15376494.2020.1824284.

Wu, J. and Habibi, M. (2021), "Dynamic simulation of the ultra-fast-rotating sandwich cantilever disk via finite element and semi-numerical methods", *Eng. Comput.*, 1-17. https://doi.org/10.1007/s00366-021-01396-6.

Xu, W., Pan, G., Moradi, Z. and Shafiei, N. (2021), "Nonlinear forced vibration analysis of functionally graded non-uniform cylindrical microbeams applying the semi-analytical solution", *Compos. Struct.*, 114395. https://doi.org/10.1016/j.compstruct.2021.114395.

Yang, Y. and Mao, Y. (2023), "Effect of cross-section geometry on the stability performance of functionally graded cylindrical imperfect composite structures used in stadium construction", *Geomech. Eng.*, **35**(2), 181-194. https://doi.org/10.12989/gae.2023.35.2.181.

Ye, M., HangKong, O., Lin, Y., Ynag, Q., Xu, Q., Chen, T., Sun, L. and Ma, L. (2023), "Electron transport properties of Y-type zigzag branched carbon nanotubes", *Adv. Nano Res.*, **15**(3), 263-275. https://doi.org/10.12989/.2023.15.3.263.

Zhang, H., Zou, Q., Ju, Y., Song, C. and Chen, D. (2022), "Distance-based support vector machine to predict DNA N6-methyladenine modification", *Curr. Bioinform.*, **17**(5), 473-482. https://doi.org/10.2174/1574893617666220404145517.

Zhang, L. and Huang, Y. (2023), "Investigating the role of nano in preserving the environment with new energy and preventing oil pollution", *Adv. Nano Res.*, **15**(6), 541-550. https://doi.org/10.12989/anr.2023.15.6.541.

Zhang, P., Song, J. and Mahmoudi, T. (2023a), "Simulation and modeling for stability analysis of functionally graded non-uniform pipes with porosity-dependent properties", *Steel Compos. Struct.*, **48**(2), 235-250. https://doi.org/10.12989/scs.2023.48.2.235.

Zhang, R., Li, L., Zhang, Q., Zhang, J., Xu, L., Zhang, B.,... Wang, B. (2023), "Differential feature awareness network within antagonistic learning for infrared-visible object detection", *IEEE T Circuits Syst. Video Technol.*, **33**(12), 7671-7683. https://doi.org/10.1109/TCSVT.2023.3289142.

Zhang, X., Li, J., Cui, Y., Habibi, M., Ali, H.E., Albaijan, I. and Mahmoudi, T. (2023c), "Static analysis of 2D-FG nonlocal porous tube using gradient strain theory and based on the first and higher-order beam theory", *Steel Compos. Struct.*, **49**(3), 293-306. https://doi.org/10.12989/scs.2023.49.3.293.

Zhang, Y., Wang, Z., Tazeddinova, D., Ebrahimi, F., Habibi, M. and Safarpour, H. (2021), "Enhancing active vibration control performances in a smart rotary sandwich thick nanostructure conveying viscous fluid flow by a PD controller", *Wave Random Complex Med.*, 1-24. https://doi.org/10.1080/17455030.2021.1948627.

Zhang, Z., Du, J. and Mahmoudi, T. (2023d), "Green synthesis of silver nanoparticles to the microbiological corrosion deterrence of oil and gas pipelines buried in the soil", *Adv. Nano Res.*, **15**(4), 355-366. https://doi.org/10.12989/anr.2023.15.4.355.

Zhao, H., Wang, H., Niu, B., Zhao, X. and Xu, N. (2024), "Adaptive fuzzy decentralized optimal control for interconnected nonlinear systems with unmodeled dynamics via mixed data and event driven method", *Fuzzy Sets Syst.*, **474**, 108735. https://doi.org/10.1016/j.fss.2023.108735.

Zhao, S., Liang, W., Wang, K., Ren, L., Qian, Z., Chen, G., Lu, X., Zhao, D., Wang, X. and Ren, L. (2023), "A multiaxial bionic ankle based on series elastic actuation with a parallel spring", *IEEE T Ind. Electr.*, 1-13. https://doi.org/10.1109/TIE.2023.3310041.

Zhou, C., Zhao, Y., Zhang, J., Fang, Y. and Habibi, M. (2020), "Vibrational characteristics of multi-phase nanocomposite reinforced circular/annular system", *Adv. Nano Res.*, **9**(4), 295-307. https://doi.org/10.12989/anr.2020.9.4.295.

Zou, Y., Zhong, M., Li, S., Qing, Z., Xing, X., Gong, G., Yan, R., Qin, W., Shen, J., Zhang, H., Jiang, Y., Wang, Z. and Zhou, C. (2023), "Flexible wearable strain sensors based on laser-induced graphene for monitoring human physiological signals", *Polymers*, **15**(17). https://doi.org/10.3390/polym15173553.

JL